Bull. Nov. Comp. Center, Num. Model. in Atmosph., etc., 10 (2005), 55–75

Numerical modeling of the Japan Sea: preliminary results*

G.A. Platov, E.N. Golubeva

Abstract. The numerical modeling of the Japan Sea seasonal variation was performed by means of the regional ocean circulation model designed in the Institute of Computational Mathematics and Mathematical Geophysics (Novosibirsk, Russia) with a simple data assimilation scheme. The aim was to get a better understanding of the Japan Sea dynamics and thermodynamics on the basis of an available GDEM dataset of climatological temperature and salinity annual variations. This paper outlines the model capability to reproduce most of the known circulation features and provides a resulting view of deep water circulation.

1. Introduction

The circulation pattern in the Japan Sea (JS) resembles the most prominent features of the global ocean and includes cyclonic and anticyclonic gyre systems, a western boundary current that separates from the coast, and a deep homogenous water mass [9]. There are also such phenomena as wind and thermahaline driven circulation, deep convection, and a variety of mesoscale eddies.

This paper aimed at better understanding of the Japan Sea dynamics and thermodynamics on the basis of available GDEM dataset of climatological temperature and salinity annual variations. The GDEM dataset suffers from a lot of artifacts and therefore cannot be used to analyze the matter without any improvements. The most appropriate instrument to get best of the available data is the numerical model capable to assimilate them and to reconstruct them in case they are coming in any sort of dynamical or thermodynamical uncertainty. Moreover, it is able to derive a circulation pattern from this data in a most natural way.

The circulation in the JS experiences the influence of the Pacific Ocean by the inflow through the Tsushima Strait and the outflow through the Tsugaru and the Soya Straits. Although these straits are rather shallow (less than 200 m), they have a profound impact on the circulation features within the JS.

*Supported by the Russian Foundation for Basic Research under Grant 02-05-64956. We also appreciate the funding from "A Study on the Monitoring of the Global Ocean Variability with ARGO Program" supported by Meteorological Research Institute / Korean Meteorological Administration. We thank our sponsors who made this investigation possible.

The sea has the subtropical and the subpolar circulation bounded by the subpolar front, similar to the open oceans. The Tsushima Warm Current (TWC), flowing from the East China Sea, supplies the salty and warm water into the basin through the Tsushima Strait. According to the available knowledge, this current splits basically into three distinct branches after entering the basin. But highly variable spatial and temporal characteristics of the TWC make it difficult to provide a solid background for such an understanding of a TWC branching pattern. Nevertheless, generally three branches are considered: the Nearshore Branch (NB), the Offshore Branch, and the East Korean Warm Current (EKWC). The latter is considered to be the western boundary current in the subtropical circulation in the JS [37].

The counterpart in the subarctic circulation is the Liman Current, which flows south to southwestward along the Russian and the North Korean coasts. Both currents contact each other around 38–40° N west of 132° E. The North-Western part of the JS as a place of mixing of these two different water masses exhibit a high eddy activity. The typical scale of eddies is about 35–80 km [21].

All this water mixture flows eastward along the Subpolar (subarctic) front (SPF) at about 40° N up to the Tsugaru Strait. The SPF divides the JS into two parts: the southern part affected mainly by the TWC branches and the northern gyre system. Part of the SPF waters flows through the strait to the Pacific Ocean while the other turns to the north contributing warm and salt waters to the northern gyre. Flowing along 44° N, a belt of this warm and salt water distributes from Hokkaido to the west (up to 131° E or so). According to [1], the deep water of the JS is formed in the process of cooling this water on the whole way from Hokkaido to the North-western region. We are going to trace this mechanism in our modeling results to give some numerical estimations.

A series of the CREAMS expeditions have detected more details of the water mass subsurface structure north of the SPF. In the upper 200 m layer, there is a salinity high sitting at the shelf break around 50–100 km off the Russian coastline. The low salinity water along the Russian coast extends from the Tatar Strait to the North Korean coast in the form of a low salinity belt [28]. The Amur river supplies fresh water into a low salinity belt through the Tatar Strait. According to Yakunin [36], the Amur river and the Okhotsk Sea contribute around 1100–1800 m^3/s of fresh water flowing along the western side of the strait, while 900–2000 m^3/s go from the JS northward along the eastern mouth of the strait as a relatively salty water. The water from the Amur river and the Okhotsk Sea encounters a strong tidal mixing with the salty water originating from the Tsushima Warm Water around the Tatar Strait and then feeds the coastal current associated with the low salinity water belt along the Russian coast.

The low salinity water south of the high salinity region is a reflection of a horizontal low salinity tongue along the SPF, sometimes extending from 131.5° E to 135° E [1].

Another problem, on which we are going to focus our attention, is the seasonal variations accompanied by the variability of an inflow/outflow system. The Tsushima current has a mean transport of about 2 Sv [35]. The overall seasonal variation appears to have an amplitude range of 0.7 Sv, with a maximum transport in November–December and a minimum in March–April. This is made up of 1.3 Sv variation in the western channel and an out-of-phase 0.6 Sv in the eastern channel [12]. The relative contributions of baroclinic and barotropic components can greatly vary. In summer, the inflow is strongly stratified due to the surface heating and an increased freshwater inflow; in winter, it tends to be vertically well mixed. Moreover, the warm water anomalies are intermittently found in the eastern channel of the Strait, which is due to the warm water intrusions from the Kuroshio [30].

Using the ADCP (Acoustic Doppler Current Profiler) data, Katoh [14] estimated that the transport of the EKWC amounted to about 1.54 Sv in June 1998, 0.70 Sv in August 1998, and 1.77 Sv in June 1989. Tanioka [33] argues that 80–90 % of the volume transport of the EKWC returns southward around the Ulleung Island forming the Ulleung Warm Eddy (UWE). The UWE is located in the central part of the Ulleung Basin (where the depth exceeds 1500 m) and has a diameter of approximately 150 km.

Observations [7, 22, 25] suggest that on average, the EKWC has a transport of ≈ 1.5 Sv and a speed of ≈ 25 cm/s, while the NKCC has a transport of ≈ 0.5 Sv and a speed ≈ 5 cm/s. Using the ADCP data collected during June-July 1999, Ramp et al. [23] computed a transport of 1.45 Sv for the EKWC and a transport of 0.78 Sv for the NKCC. Note, however, that these values change in various time spans. It is important to realize that, for the time period considered by Ramp et al. [23] no UWE was observed.

Seasonal and main thermoclines are very shallow in the JS and most of the sea is occupied with nearly homogeneous water colder than 1 °C, which has been known as the Japan Sea Proper Water (JSPW). Sudo [29] and Senjyu and Sudo [26] found a discontinuity in vertical profiles of potential temperature and dissolved oxygen from a highly selective CTD or hydrographic data and suggested a possible thermohaline circulation. A water mass with a vertical salinity minimum (< 34.06 psu) called the Japan Sea Intermediate Water (JSIW) is found below the TWC at the subsurface (200–400 m) with a density range, roughly $26.9 < \sigma_\theta < 27.3$ in the Ulleung Basin and the adjacent area. This water mass contains a relatively high oxygen concentration, suggesting that it originates from the descending surface water renewed by the winter convection somewhere north of the SPF. The strong thermocline at around 200 m depth is the boundary between the TWC and the JSIW [16, 17].

Finally, we will make some notes on the deep water circulation analysis. Yet little is known on the horizontal distribution of temperature and salinity in the deep water, because their horizontal variation is too small to be well resolved. This character makes it difficult to deduce the deep flow field from the dynamical calculation. Therefore, the flow in the abyssal JS has been mainly deduced from the water property distributions [26, 27]. On the other hand, direct measurements with a moored current meter were carried out in the JS, and the long-term moorings in the JSPW were frequently made in the last 10 years. Takematsu et al. [31, 32] performed the direct current measurements at seven stations in the Japan Basin and revealed a vertically coherent structure of the flow field in the JSPW. Nowadays, the number of direct observational data on deep currents is rapidly increasing. Senjyu et al. [27] analyzed the long-term current measurements carried out with the CREAMS programme under the main thermocline deeper than 500 m in the period from 1986 to 1999. The estimates of the deep flow field in the JS area were performed applying the variational method to the observed field. The flow configuration is characterized by the cyclonic circulation along the basin periphery and a weak current in the interior regions. Relatively strong currents exist in the eastern and western parts of the Japan Basin, around the Yamato Rise, and the southern part of the Yamato Basin. The cyclonic subarctic circulation in the Japan Basin 40° N is intensified in February as compared to that in August; in particular, the south-westward currents along the Russian coast are strengthened. This winter spin-up of the subarctic gyre is found in the numerical model experiment made by Kim and Yoon [15] and they attributed it to the positive wind stress curl associated with the winter monsoon blowing from the Asian continent.

The GDEM dataset [34] was adopted to set up the initial and open boundary conditions as well as to provide a source of data to be assimilated. The primary source of this data is the MOODS (Master Oceanographic Observation Data Set) containing about 7 million observations worldwide.

However, analysis shows a poor quality of these data. The vertical static instabilities are especially intrinsic of the resulting density field for the layers deeper than 500 m. Extensive editing is required to remove anomalous features caused by oceanographic studies of transient features such as rings, by poor observations, by using data collected during many years, and by variations within a season.

2. Numerical methods and the JS model

First we tried to run POM [2], but we were not able to produce a reasonable current field. The matter was not investigated thoroughly, but it was proved that the major factor is that POM falls to describe horizontal diffusion over

such a long period of integration (years). The diffusion along sigma isosurfaces, especially, at a shelf break contributes to false downwelling favorable gradients and finally leads to formation of strong artificial currents there. The strength of the northern gyre caused by this factor was sometimes equal to 30–40 Sv, which is extremely impressive, and it was distributed from top to bottom with nearly a constant speed value. That is why finally we decided to imply z-level model, which is free from this problem.

2.1. Model

The finite element model designed at the Institute of Computational Mathematics and Mathematical Geophysics by Kuzin et al. [5,6,18] was adopted to conduct a series of numerical experiments. Among two variants of this model (sigma- and z-coordinates) the one with z-coordinate system was chosen. The reason for such choice is explained above.

The model equations are formulated in spherical coordinates. The prognostic variables are: potential temperature, salinity and two horizontal velocity components. The vertical velocity, which is a diagnostic variable, is obtained from the continuity equation.

The primitive equations are simplified by introducing the hydrostatic approximation and the Boussinesq approach. The horizontal diffusion and viscosity is a Laplacian operator. The rigid lid approximation is applied at the surface.

A set of momentum equations is solved in three steps. First, the advection-diffusion terms are processed. Then, the resulting velocity field is assumed to consist of the two modes: barotropic and baroclinic. The barotropic mode velocity is obtained from the linear streamfunction equation. The right-hand side of this equation includes the vertical average of the momentum equations. The continuity equation is considered as an analogue of the temperature equation when a constant is used instead of the variable.

To solve the 3D equations of heat and salt transport, a splitting up technique is adopted by processing each coordinate direction consecutively. The splitting algorithm is described in [6]. The numerical scheme for the advective operator is obtained as a result of numerical diffusion subtraction from the first order up-stream difference scheme. The subtracted diffusion multiplied by some factor ranging from 0 to 1 could be used to make results more regular. In our runs, we adopted the factor of 0.125.

The density is a function of potential temperature, salinity and pressure. The equation of state is taken from [4].

All the solid lateral boundaries and the ocean floor are insulating for temperature and salinity. A no-slip condition is applied for the horizontal velocity components along the lateral boundaries. At the ocean bottom,

a linear drag condition is specified for the momentum to include the bottom friction effect. On the open boundaries, the flow is considered to be a barotropic one with a prescribed transport (see, further, Section 2.2.2). Temperature and salinity fields are allowed to be transported outside the domain, while in the case of the inflow the prescribed climatological values are specified to be advected in.

The surface air-sea fluxes are further described in Section 2.2.4.

The convective and wind-driven vertical mixing is parameterized according to [19]. The vertical turbulent coefficient is taken in the form

$$A_z = (ch)^2 \sqrt{\left(\frac{\partial u}{\partial z}\right)^2 + \left(\frac{\partial v}{\partial z}\right)^2 - \frac{g}{\rho}\frac{\partial \rho}{\partial z}},$$

which is applied in instability layers where the expression under the square root sign is positive (u, v are horizontal velocity components, ρ is a potential density, g is a gravity constant, and h is a vertical thickness of an instability layer).

2.2. Model configuration

2.2.1. Horizontal diffusion and viscosity. The results of the Naval Research Laboratory Layered Ocean Model (NLOM) [13] elucidate the impact of the eddy variability on the EKWC separation from the Korean coast. The eddy variability is suppressed by either increasing the model viscosity or decreasing the model resolution. The simulations with a decreased eddy variability indicate to a northward overshoot of the EKWC. Only the model simulation with a sufficient eddy variability depicts the EKWC separating from the Korean coast at the observed latitude. We started with a constant viscosity and diffusion coefficients with a value of 100 m^2/s. The result was like those predicted by Jacobs et al. [13] with the EKWC overshooting up to 41–42° N latitudes leaving no space for the NKCC. Using the NLOM, Jacobs et al. were able to produce a better EKWC separation when they used the eddy viscosity equal to 5 m^2/s and 1/32° spatial resolution. The implication of these parameters could result into a significant time step limitation, which was not desirable. So, we settled up on the solution that the model resolution is to be a bit poorer with 0.05° spacing and, also, the Smagorinsky parameterization of eddy viscosity was applied with a minimum value of 5 m^2/s. Then we were able to use a time step of 30 minutes. Nevertheless, further implication of an additional filtering procedure allowed us to increase this value up to 1 hour. Another way to obtain a proper EKWC separation is (according to [15]) to utilize an isopycnal diffusion, although it does not seem to be necessary as we were able to produce the same result without this sort of diffusion. Also, one of the proposed ways to obtain a more realistic current feature is to support small-scale topographic eddies

Table 1. List of model configuration parameters

Parameter	Value
Horizontal resolution	$dx,\ dy = 0.05^\circ$
Time step	$dt = 3600$ s
Minimum depth	$h_{\min} = 20$ m
Minimum viscosity	$A_{\min} = 5.0$ m^2/s
Maximum viscosity to switch on an additional filter	$A^* = \text{horcon}\frac{dx \cdot dy}{dt}$
Coefficient in the Smagorinsky parameterization	horcon $= 0.005$
Relaxation time scale and time lag	$\tau = 37$ days
Temperature variation amplifying coefficient	$r = \cos^{-1}(2\pi\tau/t_{\text{year}}) \approx 1.25$

by reducing a barotropic viscosity term. The idea was introduced by Holloway in [11] and is adopted — as an additional model option — to investigate this problem in future runs. Our implication of this approach alone without increased resolution and low viscosity was not able to attain a better EKWC separation, although it produced some significant result improvements elsewhere in the region, while used with 0.1° resolution and 100 m^2/s viscosity/diffusion coefficient. The final list of the key model parameters is summarized in Table 1.

2.2.2. Strait transports. The model domain covers the whole of the Japan Sea, and there are four straits included as open boundaries. The first is Tsushima (Korean) Strait, which is divided by the Tsushima Island into two parts: eastern and western throughflows. The next strait is the Tsugaru Strait separating Honshu and Hokkaido Islands. The Soya Strait (Strait of La Perouse) is another along with the Tsugaru Strait outflow channel. The northern boundary with the Tatar Strait is considered to be closed with zero transport through it. All transports are calculated in the following time-dependent form:

$$\text{Tr}(t) = \overline{\text{Tr}} + \delta\text{Tr}\cos\left(\frac{2\pi(t - t_0)}{t_{\text{year}}}\right), \tag{1}$$

where Tr is the resulting transport, $\overline{\text{Tr}}$ is the annual mean transport, δTr is an amplitude of its seasonal variation, t_0 is the reference time of the annual maximum, t_{year} is the year cycle as if consisting of 360 days.

The Soya Strait outflow transport value is adopted to be equal to the residual of all other inflows/outflows. The adopted parameters of the straits are listed in Table 2. They are taken according to [12].

2.2.3. The vertical resolution. The bottom topography is based on ETOPO5 bathymetry interpolated onto the model grid. The resulting depth value at each grid node was then substituted by the nearest available vertical level of the model. The vertical spacing is defined by 27 model levels: 0,

Table 2. The adopted parameters of straits

Strait	$\overline{\mathrm{Tr}}$, Sv	δTr, Sv	t_0, day
Tsushima Strait (West)	1.28	0.65	315
Tsushima Strait (East)	0.72	0.30	135
Tsugaru Strait	1.26	0.10	330
Tatar Strait	0	0	—

10, 20, 30, 40, 50, 65, 80, 100, 125, 150, 200, 250, 300, 400, 500, 600, 700, 800, 1000, 1250, 1500, 1750, 2000, 2500, 3000, 3500 m. The depth minimum over the shelf region is set equal to 20 m. This means that if a real depth is less than this value, then it was deepened down to reach this magnitude. Choosing this value assures that there are at least three model levels present at each grid node.

2.2.4. Forcing and data interpolation. The monthly mean temperature and salinity from the GDEM dataset [34] were adopted to produce a "nudging" forcing. Both temperature and salinity were first interpolated horizontally onto the model grid at each vertical data level by means of

$$\psi(x,y) = \sum_i W_i \psi_i \Big/ \sum_i W_i, \tag{2}$$

where ψ is any evaluated variable, W_i are weight coefficients, i numbers the data points connected to one at (x,y). Two points are not considered connected if the direct line between them crosses some natural barriers like a shore line, an island, an underwater ridge, etc. The weight coefficients W_i depend on the distance between connected points. If the distance is $r_i = \sqrt{(x-x_i)^2 + (y-y_i)^2}$, then

$$W_i = \exp\left(-\frac{r_i^2}{4R^2}\right), \tag{3}$$

R is the search radius, it is adopted to be $R = 1/4°$, while the GDEM data are presented with $1/6°$ resolution. The data produced that way are used directly only in setting the lateral boundary conditions for temperature and salinity. The annual mean temperature and salinity are also used to initialize these fields. In addition, the produced fields T and S are the source of additional forcing applied according to a "nudging" technique. To some extent this utilization could be referred to as data assimilation.

The vertical interpolation uses the cubic splines and, if needed, data are extrapolated downward by setting a constant value taken from the deepest available observation.

The same procedure is used to obtain a horizontal interpolation of both wind stress components. The wind stress was provided by Na's dataset [20].

The only difference here is that search radius was taken equal to 0.75° because the original wind stress data resolution is only $0.5 \times 0.5°$.

2.2.5. Nudging. The vertical heat and salt fluxes are considered to have zero values. The real heat and salt income is contributed through the arrangement of the "nudging" assimilation. According to the "nudging", idea an additional relaxation term was adopted in temperature equation in the form

$$\left(\frac{\partial T}{\partial t}\right)_{\text{nudging}} = \gamma(z)(T^*(t-\tau) - T), \tag{4}$$

so that the model is nudged towards T^* — the temperature produced using the interpolated GDEM temperature T_{GDEM}:

$$T^* = \overline{T_{\text{GDEM}}} + r(T_{\text{GDEM}} - \overline{T_{\text{GDEM}}}), \tag{5}$$

where the overbar means the annual averaging and r is an amplifying factor. In (4) γ is the relaxation coefficient. Its vertical distribution is established by

$$\gamma(z) = \begin{cases} \tau^{-1}, & \text{if } z > -500 \text{ m} \\ 0, & \text{otherwise,} \end{cases} \tag{6}$$

where τ is the relaxation time scale and is the same as the time lag in (4). Its value is chosen according to Holland [10] to be equal to 37 days, although he used it only to specify surface boundary conditions. The amplifying coefficient r is approximately equal to 1.25. This value is evaluated from the fact that if the time dependence of temperature T^* were

$$T^*(t) = \overline{T^*} + \delta T^* \cos\frac{2\pi(t-t_0)}{t_{\text{year}}}, \tag{7}$$

then the solution of

$$\frac{\partial T}{\partial t} = \frac{1}{\tau}(T^*(t-\tau) - T) \tag{8}$$

would be $T(t) = T^*(t)$ only in case of $r = \cos^{-1}(2\pi\tau/t_{\text{year}})$.

The salinity is treated the same way as temperature.

The original GDEM data look most doubtful for the deep layers starting from 500 m. Therefore, we are not keen to nudge the solution toward them at deeper layers. If we do, it would take a long time of numerical integration to reach any stabilization of deep ocean circulation. On the contrary, for the upper layers, the relaxation time toward quasi-stable state is shorter and we are going to reach the stable seasonal variations and to analyze the resulting dynamics. The main priority in our study is the resulting current system corresponding to available temperature and salinity data. That is why we extend nudging procedure to 500 m instead of applying it at the sea surface. Thus we lower the role of the numerical model down to the role of an instrument allowing to get better interpretation of the available data.

2.2.6. Model run. The numerical experiments basically consist of two periods:

1. Diagnostic two-year run with temperature and salinity evolving in time forced only by the nudging term as in (8), i.e., no diffusion, no advection, no any other terms are applied. Basically, one-year run is enough to attain a quasi-equilibrium state, the only reason why the second year is needed is to produce the complete year-round diagnostic results.
2. Prognostic run with temperature and salinity normally evolving in time. The length of this period depends on the difference measure between two subsequent years. It could be evaluated in terms of the mean kinetic energy or a maximum temperature deviation, etc.

According to these two periods, the model experiences two shocking events: the first is when the model dynamics adapts to prescribed density gradients, while the second is when the density itself starts to evolve according to the above dynamics. In the first case, the pressure gradient term is ramped from zero over the period of 30 days, while in the second case the same ramping is applied to temperature and salinity advection (convection) terms.

3. Results

3.1. Diagnostic spin-up

The model attains the quasi-equilibrium state pretty fast (see the energy chart) with further periodical development reflecting a seasonal variation. The resulting stream function resembles some dynamic features produced by the p-vector method [3, 24]. The most prominent feature standing beyond a commonly accepted circulation pattern is the northward water motion along 133°E longitude. This feature is also present and overestimated in our diagnostic results. It appears in the form of a dipole of positive and negative vorticity there. The fact that it completely disappears during the following prognostic calculations indicates that it could be just an inconsistency of the GDEM data which were used here and in both above-mentioned cases.

3.2. Horizontal viscosity/diffusion and filtering

During the first three years of a prognostic mode integration, we tried to apply different combinations of the horizontal diffusion along with filtering (see the energy chart in Figure 1 and the model settings list in Table 3).

After all these tests we settled upon the Smagorinsky parameterization with a 1-2-1 filter applied only at points, where the Smagorinsky viscosity coefficient is too high. For example, if velocity is directed zonally, then the Smagorinsky coefficient could be estimated as

$$A = C\,\delta x\,\delta y \frac{\partial u}{\partial x} \approx C\,\delta y\,\delta u, \tag{9}$$

where A is a viscosity coefficient, C is a proportionality constant, δx and δy are spacings along the longitude and latitude and δu is the velocity difference between two nearest points in the longitudial direction. The Courant restriction for advection demands that

$$\delta u\,\delta t \leq \delta x, \tag{10}$$

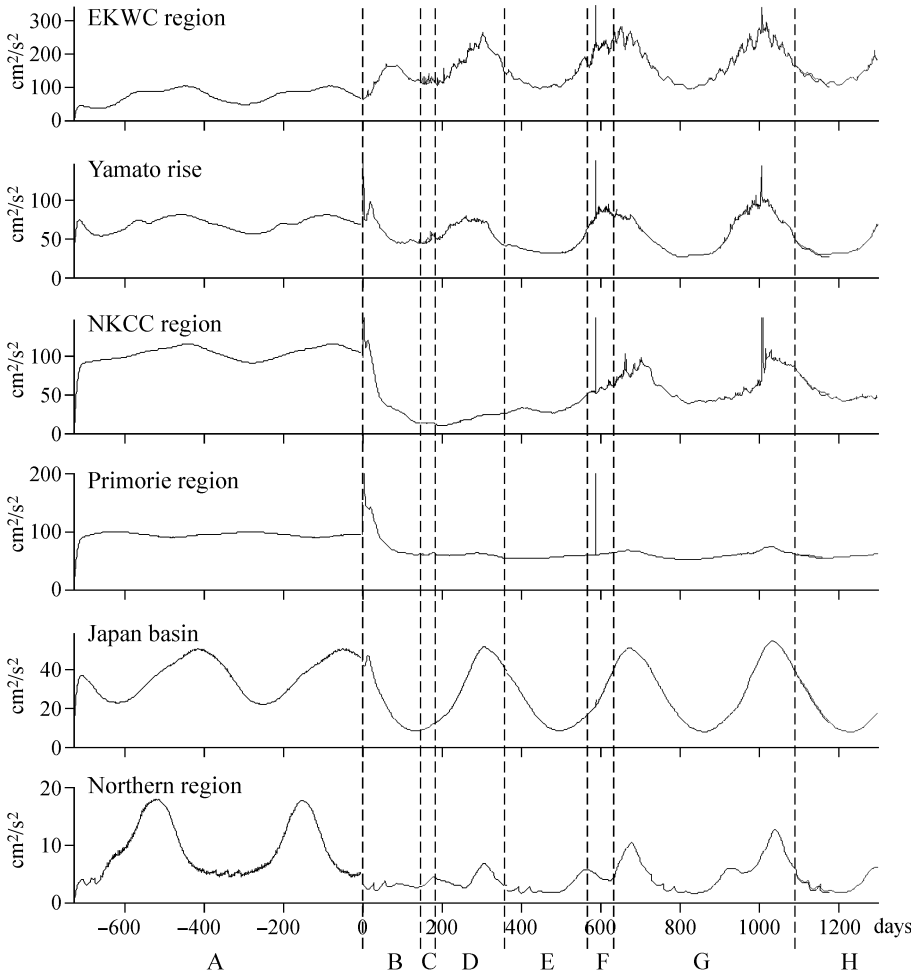

Figure 1. The kinetic energy of a unit mass (cm^2/s^2) changes during the overall model run. The time axes are labeled in days with the negative values corresponding to a diagnostic spin-up period. The panels represent the value averaged over six different regions of the Japan Sea. The periods of different model settings are labeled with Latin capital letters along the lower panel

Table 3. The development of model settings during the run

Label	The major features or changes made to previous revision	The reason why this setting was declined
A	Diagnostic mode	
B	Introduced T/S horizontal filtering and a filter for a stream function with both applied once a day	Too smooth solution
C	Smagorinsky viscosity without T/S filtering	Unstable solution
D	Fourth order T/S filtering	Too smooth solution
E	Smagorinsky viscosity updated right after a new velocity is calculated at each time step	Unstable solution
F	Introduced a selective filtering described in section 3.2 for T/S fields at each time step	Unstable solution
G	The same as F but filtering is applied right after the horizontal advection	Too smooth stream function
H	Selective filtering is applied to the stream function as well	

where δt is a model time step. Substituting δu from 9 into 10 we find that the Courant restriction turns into the upper limit for the Smagorinsky coefficient like

$$A \leq A^* = C\frac{\delta x\, \delta y}{\delta t}. \tag{11}$$

To satisfy this restriction in the case of the two-grid-point instability, at the points where A becomes greater than $\frac{1}{2}A^*$, we apply a 1-2-1 filter which is implicit in contrast to the model viscosity/diffusion scheme (it is explicit). The lower level of the viscosity coefficient is set equal to $A_{\min} = 5\ \mathrm{m}^2/\mathrm{s}$.

3.3. Prognostic setup

After allowing temperature and salinity fields to evolve with time, the stream function dramatically changes. The above-mentioned dipole structure starts changing. Its maximum moves eastward also getting lower during this motion. The minimum stretches are zonally becoming not that low as in the diagnostic mode. The East Korean high appears and grows until it ends up with a strong and narrow East Korean Warm Current. Its separation point moves gradually northward from the Tsushima splitting point up to 37–38° N. When it reaches its final position, the stream function high corresponding to the former dipole maximum disappears completely, its counterpart — low stretches — the whole-wide zonally occupying the northern part of the Japan Sea.

The deep water salinity becomes more uniform concentrating around the value 34.08 psu. Perhaps, this is an indication to a poor quality of the original salinity data, presuming that the deep water salinity measurements are occasional and hence are more dependent on the situation they were taken,

while the upper layer salinity is more reliable because its measurements are more frequent and cover the whole lot of climatological situations.

3.4. Seasonal circulation features

Since the maximum Tsushima transport according to [35] corresponds to the winter time (November–December), then the middle of November (the time of our model maximum transport) will be later referred to as winter, and the comparison will be made with the middle of May (a minimum transport period). It should also be noted that the core of the winter inflow occurs through the western part of the Tsushima Strait, while during summer its core is shifted towards the eastern throughflow.

The Tsushima Strait, the Tsugaru Strait and the Soya Strait are all not deeper than 100–200 m. This means that waters coming in and out are generally of the surface water type. Although the influence of this throughflow across the whole Japan Sea is significant, the surface water type is also affected a lot by the internal forcing. The manifestation of that fact is the resulting picture of the barotropic current system shown in terms of a stream function in Figure 2. Along with the stream lines connecting the inflow with outflows, it also contains at least two internal loops which could be forced by the internal factors only. The overall current structure looks similar to the global circulation pattern. It consists of two circulation cells. The most prominent one is the northern gyre corresponding to the subpolar gyre system. The southern part is represented by the relatively strong western current — East Korean Warm Current, which separates at about 37–38° N driving its water to the east along the subpolar front.

The driving mechanisms in a similar global circulation pattern are the trade wind in the south and the zonal westerly wind along the subpolar front, both being regular features and as a response to that forcing a strong anticyclonic circulation spreads oceanwide from the equator up to the middle latitudes at about 40° N. The weak easterly winds are blowing over the northern part of the Atlantic and the Pacific oceans thus forming the subpolar gyre system. The Stommel western intensification applied to these northern gyres ends up with such strong currents as the Oyashio in the North Pacific and the Labrador current in the North Atlantic.

Another factor supporting this circulation pattern seems to be a zonal heating difference giving rise to the eastward water transport in the middle. This feature reflects the fact that the cold subpolar water and the warm equator water (provided that salinity is almost constant) form the global density and pressure gradients responsible for the geostrophic eastward water motion. This factor supports the eastward motion along the subpolar front.

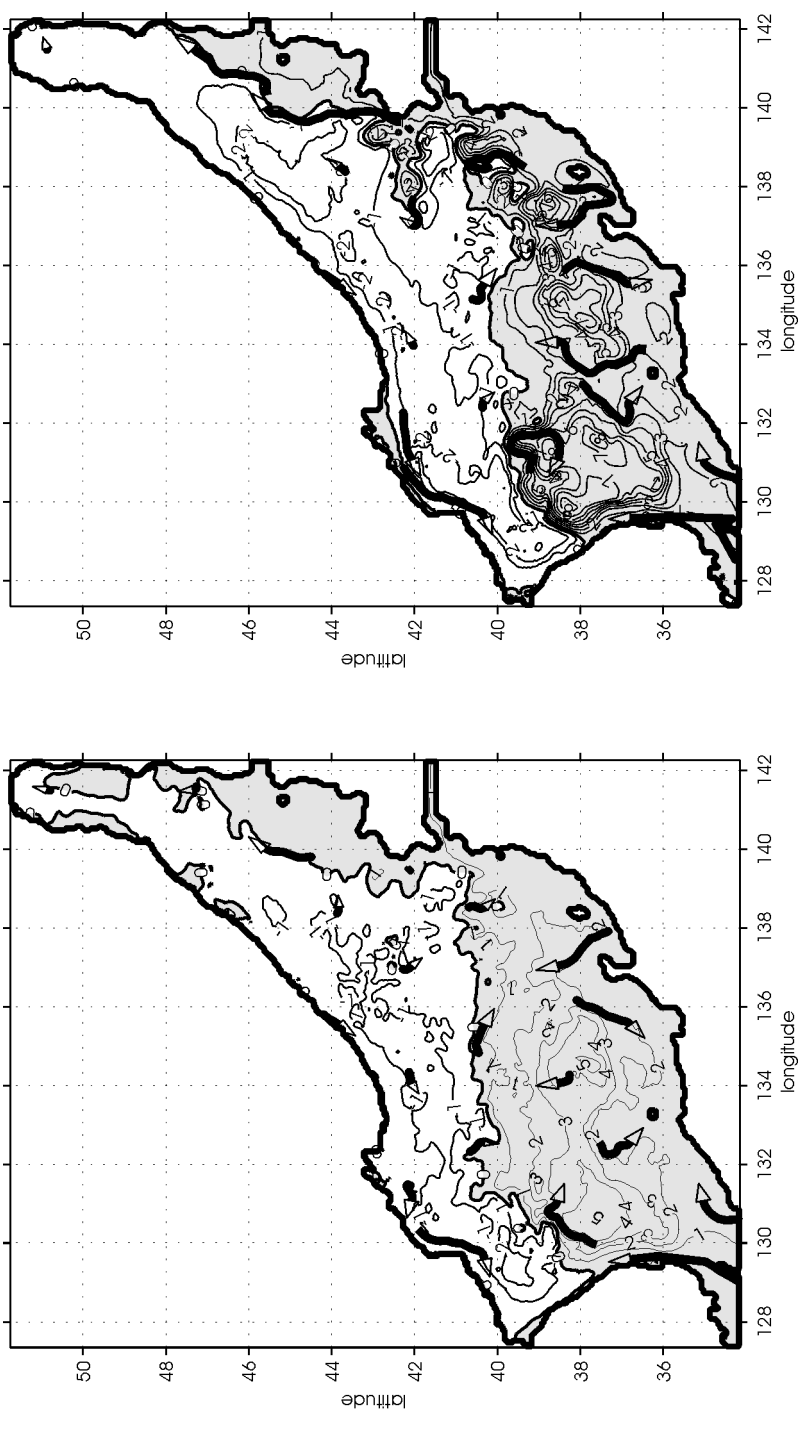

Figure 2. The resulting stream function (Sv) of a quasi-stable seasonal variation. The left panel represents the lower Tsushima transport (summer) season, the right one is the higher Tsushima transport (winter) season. The shaded area is the positive stream function area, which could roughly be attributed to the southern circulation cell, while the non-shaded area — to the northern gyre system. Arrows are plotted over to indicate the flow direction

Looking at the stream function presented in Figure 2 one could suggest that the same or similar processes are taking place in the Japan Sea although the horizontal scale is smaller and hence the Coriolis parameter variability is of less importance, so that the western currents intensification is not that prominent. The forcing mechanism seams to be the same as above but applied to the northern gyre which is driven by the westerly winds in the middle and the easterly weak or absent winds in the north shallow part. The southern part has its peculiarity. The absence of strong winds in the south, which are analogous to the trade winds, makes the southern circulation cell a bit different in comparison with the global circulation. The mid-latitude westerly winds are still present driving the subpolar front waters to the east. The southern recirculation could hardly be supported by local winds though, because they are not regular and, in general, are not anticyclonic favorable. This means that the recirculation seen in Figure 2 is more likely to be via subsurface undercurrents.

In our case, we do not apply surface heating, and its role in supporting the south-north difference is played by a relaxation term in temperature and salinity equations assimilating a seasonal temperature and salinity variations. As the above term is three-dimensional, this means that the vertical processes are less important as in the case of the surface heating, and thus the result is more dependent on the vertical structure of prescribed temperature and salinity fields rather than the simulated regular vertical motion and convective mixing parameterizations.

3.5. Deep water circulation

Figure 3a of the averaged velocity in the layer of 600–1000 m shows generally strong boundary currents along the western side of the northern portion of the Japan Sea with weaker flows in the interior of the basin and along the eastern boundary. This supports the conclusion made in [8] on the basis of more than 30 PALACE floats in the northern portion of the Japan Sea. In winter, the temperature difference between the sea surface and 800 m in Figure 3b shows that water column is almost well-mixed along the western boundary, especially, in the vicinity of Peter the Great Bay. This result contributes to the idea of a deep convection in this region. Strength of the convective overturning determines the high intensity of the subpolar front just to the south of this area. In the southern portion of the Japan Sea, the flows are generally following the coastal slope from the Hokkaido in the east to the Ulleung basin in the west.

In the east, as is seen from the zoom plot in Figure 4b, these flows are highly irregular and consist of a series of cyclonic and anticyclonic eddies. Nevertheless, the offshore side, following latitudes 40–41° N, represents a weak but steady eastward transport. In the west, Figure 4a, although there

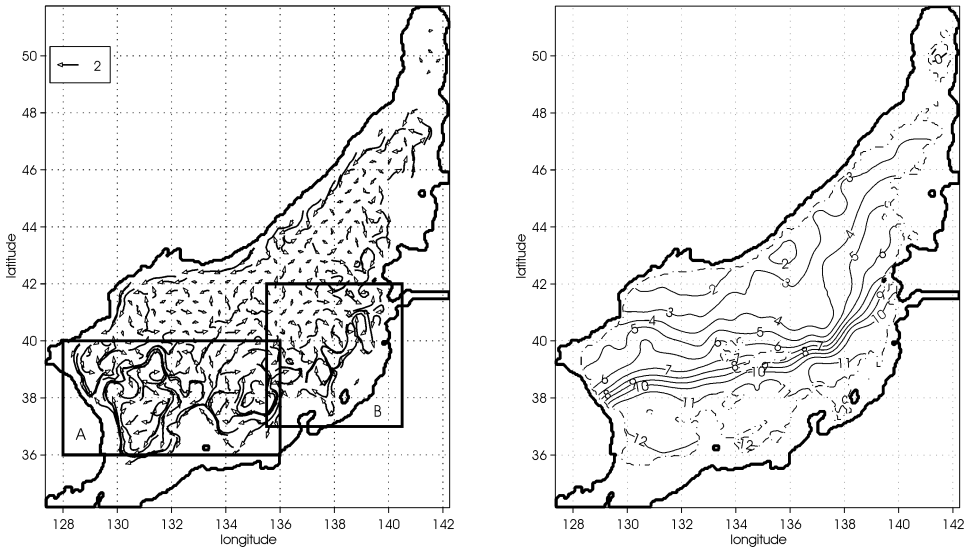

Figure 3. Deep water circulation pattern in winter: a) the vertically averaged velocity in 600–1000 m layer and b) the temperature difference between sea surface and 800 m depth

is a lot of small-scale eddies, the overall transport is anticyclonic with a westward motion along the shelfbreak and an eastward motion in the middle of the basin, corresponding to the SPF position.

4. Discussion

The described model developed to simulate the JS circulation pattern seems to be capable of reproducing the most prominent dynamic features. To be more assured in this conclusion, we need to increase model resolution to see that most results obtained so far will not be significantly changed after that. The most prominent thing that we can confirm according to our current results is the following: to depict the most prominent JS circulation features by means of numerical modeling, one needs to increase the model resolution up to about 5 km and to decrease model viscosity down to 5 m^2/s for the most of the simulated area. These conditions could be even stronger, as in our tests we also applied a "nudging" scheme that forced the model temperature and salinity field not to go far from the prescribed ones. As one can see, we did not use an isopycnal diffusion, so it is not as necessary to apply as it is sometimes believed.

The details of the above described deep circulation obtained as a result of numerical modeling are to be confirmed by further studies and model development. The main difficulty is to obtain the reliable temperature and

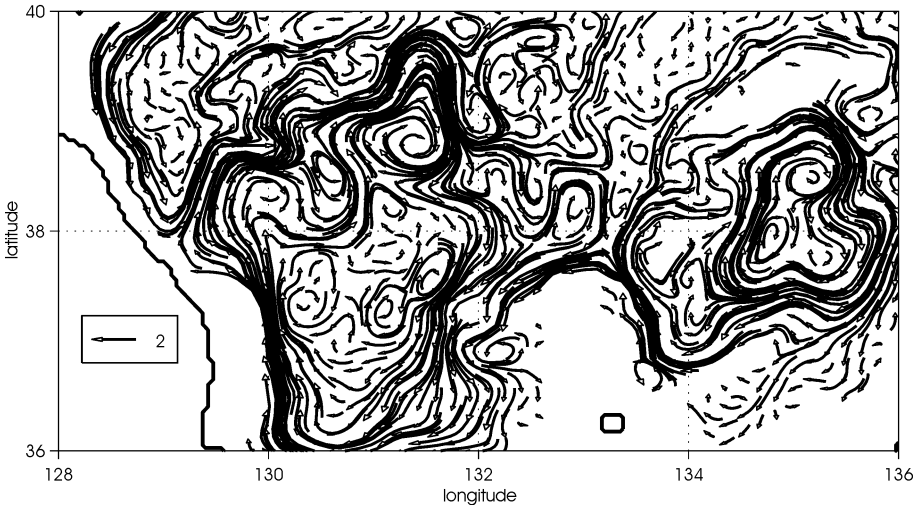

a

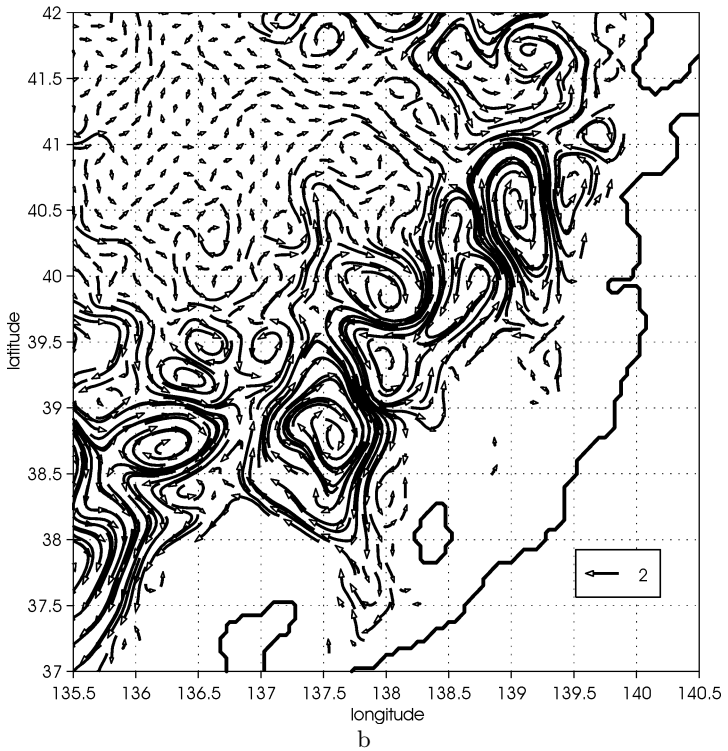

b

Figure 4. A close view at the deep water circulation pattern in winter in areas A and B specified in Figure 3a: the vertically averaged velocity in 600–1000 m layer

salinity data. The deep water properties are almost homogeneous and the dynamics restored by means of numerical simulation is more dependent on the assimilated data precision. In this circumstances the most promising way to obtain a deep water circulation pattern is believed to design a more sophisticated assimilation scheme along with an excessive number of real-time direct measurements. Two ways of obtaining these data excess are most intensively developed at the moment. The first is the satellite measurements and the second is a growing number of drifters deployed accordingly projects like ARGO, etc. The Japan Meteorological Agency is now capable to provide daily satellite images of temperature and sea level anomalies distributions in the JS and make them available for a wide scientific community. This stimulates the real-time model simulation, although the results which could be obtained this way can hardly be used to make some general conclusion about the JS climatology, because they are situation-dependent. To do such conclusions, we need at least several decades of detailed measurements, while at the moment, there are available only series of about ten years. The drifter measurements, although their number is growing, are still scarce and probably could be used only to verify real-time model results.

References

[1] Aubrey D.G., Danchenkov M.A., Riser S.C. Belt of salt water in the northwestern Japan Sea // Proc. CREAMS'2000 Intern. Symposium. — Vladivostok: Far Eastern Hydrometerological Institute, 2000. — P. 11–20.

[2] Blumberg A.F., Mellor G.L. Diagnostic and prognostic numerical circulation studies of the South Atlantic bight // J. Geophys. Res. — 1983. — Vol. 88. — P. 4579–4592.

[3] Chu P.C., Lan J., Fan C. Japan Sea thermal structure and circulation. Part I: Climatology // J. Phys. Oceanogr. — 2001. — Vol. 31. — P. 244–271.

[4] Gill A.E. Atmosphere-Ocean Dynamics. — Academic Press, 1982.

[5] Goloubeva E.N., Ivanov Ju.A., Kuzin V.I., Platov G.A. Numerical modeling of the World Ocean circulation including upper ocean mixed layer // Oceanology. — 1992. — Vol. 32, No. 3. — P. 395–405.

[6] Goloubeva E.N. On the numerical modeling of the World Ocean circulation in the sigma coordinate system // Bull. Novosibirsk Comp. Center. Ser. Num. Mod. in Atm. etc. — Novosibirsk, 2001. — Iss. 7. — P. 1–16.

[7] Gordon A.L. Sea of Japan // Marginal Seas and the Kuroshio: An Assessment of Mutual Impact / Department of Oceanography. Florida State University. — Tallahassee, 1990.

[8] Danchenkov M.A., Riser S.C. Observation of currents, temperature and salinity in the Japan Sea in 1999-2000 by PALACE floats // Proc. CREAMS'2000

Intern. Symposium. — Vladivostok: Far Eastern Hydrometerological Institute, 2000. — P. 33–40.

[9] Hogan P.J., Hurlburt H.E. Impact of upper ocean-topographical coupling and isopycnal outcropping in Japan: East Sea models with 1/8° to 1/64° resolution // J. Phys. Oceanogr. — 2000. — Vol. 30, No. 10. — P. 2535–2561.

[10] Holland W.R., Malanotte-Rozzoli P. Assimilation of altimeter data into an ocean circulation model: Space versus time resolution studies // J. Phys. Oceanogr. — 1989. — Vol. 19. — P. 1507–1534.

[11] Holloway G., Sou T., Eby M. Dynamics of circulation of the Japan Sea // J. Marine Res. — 1995. — Vol. 53. — P. 539–569.

[12] Isobe A. Seasonal variability of the barotropic and baroclinic motion in the Tsushima–Korea Strait // J. Oceanogr. — 1994. — Vol. 50. — P. 223–238.

[13] Jacobs G.A., Hogan P.J. Whitmer K.R. Effects of eddy variability on the circulation of the Japan/East Sea. — http://www7320.nrlssc.navy.mil/links/papers/jes_eddies/txt/jes_eddies.htm.

[14] Katoh O. Structure of the Tsushima Current in the southwestern Japan Sea // J. Oceanogr. — 1994. — Vol. 50. — P. 317–338.

[15] Kim C.-H., Yoon J.-H. A numerical modeling of the upper and the intermediate layer circulation as deduced from isopycnal analysis // J. Oceanogr. — 1999. — Vol. 55. — P. 327–345.

[16] Kim K.J., Seung Y.H. Formation and movement of the ESIW as modeled by MICOM. — J. Oceanogr. — 1999. — Vol. 55. — P. 369–382.

[17] Kim Y.-G., Kim K. Intermediate waters in the Japan/East Sea // J. Oceanogr. — 1999. — Vol. 55. — P. 123–132.

[18] Kuzin V.I. The Finite Element Method in the Ocean Processes Modeling. — Novosibirsk: Computing Center, 1985 (In Russian).

[19] Marchuk G.I., Kochergin V.P., Klimock V.I., Sukhorukov V.A. On the dynamics of the ocean surface mixed layer // J. Phys. Oceanogr. — 1977. — Vol. 7. — P. 865–875.

[20] Na J.Y., Seo J.W. The sea surface winds and heat flux in the East Asian marginal seas. — Hanyang University, Korea. — (Tech. Rep. / Dept. of Earth and Marine Sciences).

[21] Nikitin A.A., Dyakov B.S. Spatial structures of fronts and eddies of the Japan sea in the 90s by satellite data // Proc. CREAMS'2000 Intern. Symposium. — Vladivostok: Far Eastern Hydrometerological Institute, 2000. — P. 260–263.

[22] Preller R., Hogan P. Oceanography of the sea of Okhotsk and the Japan/East sea coastal segment // The Sea. Vol. 11 / Ed. A. Robinson and K. Brink. — John Willey and Sons, 1998. — P. 429–481.

[23] Ramp S.R., Bahr F.L., Ashjian C.J., Talley L.D. The upper-ocean circulation in the Ulleung basin during June-July 1999. — (Submitted to Deep-Sea Research II, 2002).

[24] Ro Y.-J., Smirnov S.V., Choi Y.-H. Estimation of current vectors in the East Sea based on P-vector method with climatological KODC, GDEM, WOA datasets // Proc. CREAMS'2000 Intern. Symposium. — Vladivostok: Far Eastern Hydrometerological Institute, 2000. — P. 94–103.

[25] Rostov I., Yurasov G.I., Rudyh N.I., Moroz V.V., Dmitreva E.V., Nabiullin A.A., Khrapchenkov F.F., Bunim V.M. Oceanographic Atlas of Bering Sea, Okhotsk Sea, and Japan/East Sea. — Vladivostok, 2001. — CD-ROM, POI FEBRAS.

[26] Senjyu T., Sudo H. Water characteristics and circulation of the upper portion of the Japan Sea proper water // J. Mar. Sys. — 1993. — Vol. 4. — P. 349–362.

[27] Senjyu T., Nagano Z., Yoon J.-H. Deep flow field in the Japan Sea deduced from current measurements // Proc. CREAMS'2000 Intern. Symposium. — Vladivostok: Far Eastern Hydrometeorological Institute, 2001. — P. 21–24.

[28] Seung Y. H., Yoon J.-H. Some feature of winter convection in the Japan Sea // J. Oceanogr. — 1995. — Vol. 51. — P. 61–73.

[29] Sudo H. A note on the Japan Sea Proper Water // Prog. Oceanogr. — 1986. — Vol. 17. — P. 313–336.

[30] Sugimoto T. A review of recent physical investigations on the straits around the Japanese Islands // The Physical Oceanography of Sea Straits. Series C: Mathematical and Physical Sciences / Ed. L.J. Pratt. — Dordrecht, The Netherlands: Kluwer Academic Publishers, 1990. — Vol. 318. — P. 191–209.

[31] Takematsu M., Nagano Z., Ostrovskii A.G., Kim K., Volkov Y. Direct measurements of deep currents in the northern Japan Sea // J. Oceanogr. — 1999. — Vol. 55. — P. 207–216.

[32] Takematsu M., Ostrovskii A.G., Nagano Z. Observations of the eddies in the Japan Basin interior // J. Oceanogr. — 1999. — Vol. 55. — P. 237–246.

[33] Tanioka K. On the East Korean Warm Current (Tosen Warm Current) // Oceanographical Magazine. — 1968. — Vol. 20. — P. 31–38.

[34] Teague W.J., Carron M.J., Hogan P.J. A comparison between the generalized digital environmental model and Levitus climotologies // J. Geophys. Res. — 1990. — Vol. 95 (C5). — P. 7167–7183.

[35] Toba Y., Tomizawa K., Kurasawa Y., Hanawa K. Seasonal and year-to-year variability of the Tsushima–Tsugaru Warm Current system with its possible cause // La Mer. — 1982. — Vol. 20. — P. 41–51.

[36] Yakunin L.P. On the reliable Amur river discharge through the new channel // Bull. Far Eastern Scientific Research Hydrometeorological Institute. — 1975. — Vol. 55. — P. 61–64.

[37] Yoon J.-H. Numerical experiment on the circulation in the Japan Sea. Part 1: Formation of the East Korean Warm Current // J. Oceanography Society. Japan. — 1982. — Vol. 38. — P. 43–51.

[38] Yoon J.-H., Ogata T. The influence of orography on the circulation of the Japan/East Sea // Proc. CREAMS'99 Intern. Symposium. — Fukuoka: RIAM, Kyushu Univ., 1999. — P. 120–123.